Blistering of film from substrate after action of ultrashort laser pulse

2016 J. Phys.: Conf. Ser. 774 012102

(http://iopscience.iop.org/1742-6596/774/1/012102)

Blistering of film from substrate after action of ultrashort laser pulse

N A Inogamov[1,2], V V Zhakhovsky[2,1], V A Khokhlov[1], A A Kuchmizhak[3,4] and S I Kudryashov[5,6]

[1] Landau Institute for Theoretical Physics of the Russian Academy of Scienses, Akademika Semenova 1a, Chernogolovka, Moscow Region 142432, Russia
[2] Dukhov Research Institute of Automatics (VNIIA), Sushchevskaya 22, Moscow 127055, Russia
[3] School of Natural Sciences, Far Eastern Federal University, Sukhanova 8, Vladivostok, Primorsky Krai 690041, Russia
[4] Institute of Automation and Control Processes of the Far Eastern Branch of the Russian Academy of Sciences, Radio 5, Vladivostok, Primorsky Krai 690041, Russia
[5] ITMO University, Kronvergskiy 49, Saint-Petersburg 197101, Russia
[6] Lebedev Physical Institute of the Russian Academy of Sciences, Leninsky Avenue 53, Moscow 119991, Russia

E-mail: nailinogamov@gmail.com

Abstract. The goal of the paper is to explain experimental results concerning film blistering. Tightly focused diffraction limited ultrashort optical laser pulse illuminates a small spot at a surface of a thin metal film mounted upon a dielectric or semiconductor support (substrate). Film mechanically separates from substrate and form a cupola like bump in a rather narrow range of absorbed fluences. Below this range deformations inside the spot are negligible. While above the range the hole remains in a film in the irradiated spot. The paper presents physical model starting from absorption and two-temperature state and including, first, description of conductive redistribution of absorbed heat, melting, hydrodynamics of strong three-dimensional deformations of a moving film, and, second, freezing of molten metal.

1. Introduction

Illumination by laser is very widely used as a tool for modification of a target. Here we consider the practically important case when a pulse is short and illuminated area is small. Before explaining how short and how small, few words about applications. Studies of the case with a short pulse and a small spot begin and continue in papers by Chichkov, Nakata and others [1–4]. Structures created in this way are used in nanoplasmonics, laser induced forward transfer (LIFT, laser printing) technologies, in metaoptics, advanced solar cells, for fabrication of photon crystals, hydrophobic surfaces, as well as for surface-enhanced fluorescence and Raman spectroscopy (SERS) applications, and fabrication of nanoparticles. Usually 30–60 nm thick gold film on glass or Si substrate are used. Of course, the problem with a thin film is a part of wider problem of ablation by ultrashort laser pulses considered in many works, see papers [5–10] and references given in these papers.

There are two geometrical parameters: a diameter of a spot $2R_L$ and thickness of a film d_f. The third spatial scale d_T is connected with two-temperature (2T) physics. An interplay between

electron-ion coupling and electron heat conduction defines thickness d_T of a heat affected zone in a bulk target. A film should be thinner than d_T to create a smooth cupola like bump. A smooth cupola appears if a film melts and velocities of a film after separation from substrate are of the order of few tens of m/s.

For the thicker films $d_f > d_T$ situation is more asymmetric relative to the middle plane of a film than in the thin case $d_f < d_T$. It is difficult to create the smooth cupola in the thick case. In the thick case the fluence should be adjusted to a very narrow range slightly above a thermomechanical ablation threshold to limit velocity of flight of a spallation shell. Otherwise velocities of flight are too high to allow to surface tension to stop the spallation shell before the breaking of a flying piece of a film.

Adhesion between a substrate and a film should be small to allow separation of a film as a whole before internal breaking of a film takes place. Adhesion is small for gold and silver films deposited on to glass mount. Then the separation from a substrate threshold is below the internal breaking threshold. Thus a range of absorbed fluences exists where a film separates, see discussion in [11, 12]. Duration of a pulse should be less than acoustic time scale $t_s = d_f/c_s$ for a film, here c_s is speed of sound. Combination of conditions should be fulfilled to obtain a smooth bump after irradiation.

2. Light absorption and thermal transport: analytic solution

Let's consider action of an ultrashort laser pulse (duration 0.05–1 ps, wavelength $\lambda = 532$ nm) onto a gold film $d_f = 50$ nm thick on a glass substrate. This problem corresponds to usual experimental conditions. Physical analysis begins with description of absorption of a pulse and finishes with freezing of molten gold because in our conditions the pulse is strong enough to melt a film. Absorption of a part of a laser energy takes place in a skin layer $\delta_{\rm sk} = \lambda/4\pi k = 20.1$ nm, here $n + {\rm i}k = 0.384 + 2.11{\rm i}$ and $\epsilon_1 + i\epsilon_2 = -4.3 + 1.62{\rm i}$ are refraction index and dielectric constant of gold for $\lambda = 532$ nm [13]. Reflection for a normal incidence is $R = 0.765$; transmission through a film $d_f = 50$ nm approximately is $\exp(-50/20.1) = 0.083$. Thus absorption by a film is $A = 1-0.765-0.083 = 15.2\%$. Wavelength $\lambda = 532$ nm, $h\nu = 2.33$ eV is rather near to the upper edge ≈ 2.5 eV of a d-band of an electron spectrum of gold where strong interband absorption exists. Therefore reflection is not very close to 100% as it is for the more longer wavelengths, e.g. $R(\lambda = 800\ {\rm nm}) = 0.988$ [13]. Absorption in a bulk target $A_{\rm bulk}(\lambda = 532\ {\rm nm}) = 23.5\%$ for wavelength $\lambda = 532$ nm is 20 times higher than $A_{\rm bulk}(800\ {\rm nm}) = 1.2\%$. (i) At the wavelength 532 nm and (ii) for our moderate range of laser intensities (I) the smearing of a vacuum boundary of a film during a pulse is negligible, (II) changes of dielectric constant as a result of electron heating during a pulse are moderate, therefore below we use the Fresnel absorption coefficient $A \approx 0.15$ to calculate absorbed energy. The absorbed energy is the only driver of all subsequent phenomena.

Absorption in a skin and transmission through a film are centered around the fast moving photons. They cover duration of a pulse. Pulse duration is the shortest time scale in the hierarchy of time scales. Duration of the two-temperature (2T) stage in gold is $t_{\rm eq} \sim 5$–10 ps. High electron temperature T_e decreases and becomes approximately equal to ion temperature at the end of the 2T stage. (i) Spreading of heat (accumulated in electrons) as a result of enhanced [14] heat conductance of 2T gold and (ii) electron cooling due to heating of an ion subsystem are two main processes at the 2T stage. An electron heat conduction of gold during a 2T stage creates a heat affected layer with thickness $d_T \sim 100$–150 nm few times thicker than a skin depth. This is said for the bulk ($d_f \gg d_T$) targets under homogeneous (large radius $R_{\rm opt} \gg d_T$ of laser beam) illumination, here d_T is thickness of a target.

In the case of usual experiments the thickness of a film $d_f = 50$ nm is thinner than thickness $d_T \sim 100$–150 nm for gold. This circumstance qualitatively differs the thin films $d_f < d_T$ from the bulk targets $d_f \gg d_T$. Heat absorbed locally $F_{\rm abs} = F_c \exp(-r^2/R_{\rm eff}^2)$ at the radius r in a

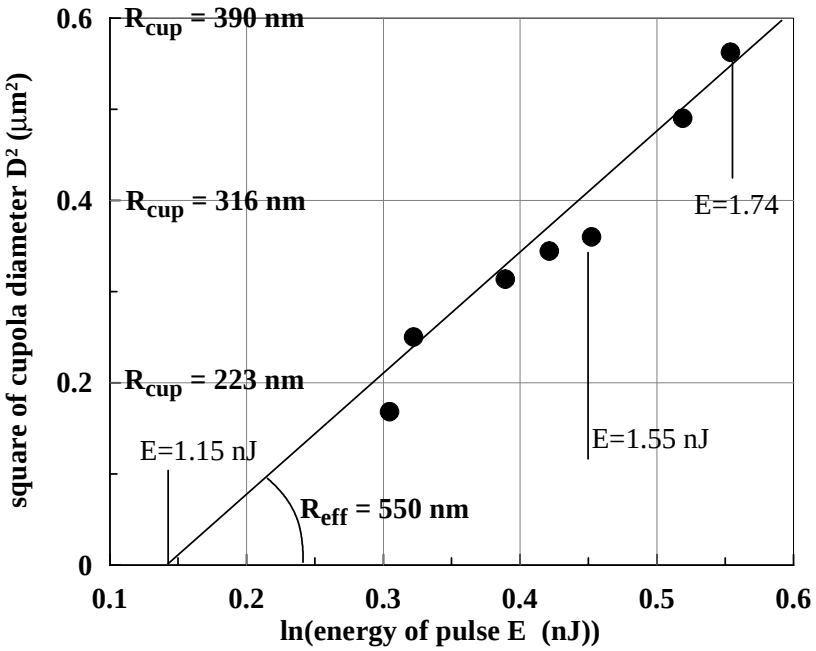

Figure 1. Experimental points are shown by black circles. Approximation given by the straight line is $D_{\rm cup}^2 = D_{\rm eff}^2 \ln(E/E_{\rm thr})$. Below the threshold energy $E_{\rm thr}$ the cupola does not appear. At the threshold $E_{\rm thr} = 1.15$ nJ the diameter of a cupola is zero. Calculation of a slope gives $R_{\rm eff} = D_{\rm eff}/2 = 550$ nm.

skin, during the time gap $t_{\rm df}^{\rm EHC} = 1$–2 ps homogenously redistributes [11, 12] along a thickness d_f from a skin. Thus electron temperature and later on ion temperature are approximately homogeneous across a thickness of a film, but remain functions of radius r. The time gap $t_{\rm df}^{\rm EHC}$ is the second shortest time scale in the hierarchy. It is shorter than duration of a 2T stage with enhanced conduction. Therefore for the tight focusing with $R_{\rm eff} \approx \lambda$ and short wavelengths λ, the 2T enhanced lateral conductance (tangentially along a film) becomes significant. It cools down the overheated electrons in the small central portion of a laser spot $\sim R_{\rm opt}$.

Let's mention that here we consider the case when we can neglect conductance of a glass substrate— all heat fluxes flow through a metal film. The role of the conducting silicon substrate at a 2T stage has to be consider separately. Main cooling and freezing of a film last much longer period of time than the 2T stage lasts. A film separates from a substrate in our applications with the hollow bumps thus a heat conductance of a substrate becomes less significant. Heat flows through a separated part of a film, and the substrate conductance influences cooling only out of a ring of a contact of a bump with a rest of a film remaining on a substrate. Comparison of experiments with a film on a glass and on a silicon shows that these two case differ slightly.

Experimental values for diameters of a cupola $D_{\rm cup}$ as a function of pulse energy are presented in figure 1. Energy distribution across an irradiated spot is $F = F_c \exp(-r^2/R_{\rm eff}^2)$. Pulse energy is $E = \int_0^\infty F(r)\, 2\pi r dr = \pi R_{\rm eff}^2 F_c$. We neglect duration of a femtosecond pulse and duration $t_{\rm df}^{\rm EHC} = 0$. In this approximation the temperature is a function of radius and time. Let us consider an evolution of a temperature profile.

Heat equation for a film thermally isolated from an underlying substrate is

$$\partial_t T = \chi\, \Delta_2 T, \quad \Delta_2 = \partial_x^2 + \partial_y^2,$$

where Δ_2 is 2D Laplacian.

This is simplified (because we suppose that a heat diffusivity χ is approximately spatially homogeneous) equation valid for the one-temperature (1T) case ($T_e = T_i = T$). For the axial-symmetric illumination, the initial and boundary conditions are

$$T(r, t = 0) = \frac{E_{\rm abs}}{\pi\, c\, d_f\, R_{\rm eff}^2}\, \exp(-\frac{r^2}{R_{\rm eff}^2}) + 300, \quad T(r = \infty, t) = 300 \text{ K}.$$

Here total absorbed and incident energies are $E_{\rm abs} = A\, E_{\rm inc}$, $A \approx 0.15$; $c \approx 3k_B n_0$ is heat capacity, k_B is Boltzmann constant, $n_0 \approx 6 \times 10^{22}$ cm^{-3} is an atomic concentration at normal conditions.

Solution of the problem is

$$T(r, t) = \frac{E_{\rm abs}}{\pi\, c\, d_f\, (R_{\rm eff}^2 + 4\chi t)} \exp\left(-\frac{r^2}{R_{\rm eff}^2 + 4\chi t}\right) + 300.$$

Exact solution of a 2T problem gradually transforming to a 1T distribution along a thin film needs a special study. We approximately estimates a role of a 2T enhancement of conductance at the time gap between the stage $t_{{\rm d}f}^{\rm EHC}$ and the end $t_{\rm eq}$ of the 2T stage. To do this we twenty times increase [14] diffusivity $\chi_{2T} = 20\chi$ at this time gap, where $\chi \approx 1.2$ cm^2/s corresponds to the room temperature. As was said, we neglect duration of the gap $t_{{\rm d}f}^{\rm EHC} = 0$. Thus at the start point $t = 0$ the temperature distribution $T(r, n, t)$ is $T(r, t)$ (homogenization across thickness d_f), here n is the direction normal to a plane of a film and a substrate. Solution at the time gap $0 < t < t_{\rm eq}$ is

$$T(r, t) = \frac{E_{\rm abs}}{\pi\, c\, d_f\, (R_{\rm eff}^2 + 4\chi_{2T} t)} \exp\left(-\frac{r^2}{R_{\rm eff}^2 + 4\chi_{2T} t}\right) + 300.$$

This solution describes fast removal of energy by an enhanced conduction from a central zone. Temperature in this expression is an equivalent ion temperature. It presents the instant local energy density per unit area

$$F(r, t) = c\, d_f\, T(r, t).$$

At the 2T stage the real ion temperature is significantly below the equivalent ion temperature. 2T two-dimensional (2T2D) problem will be solved in future to define evolution of T_e and T_i during the 2T stage. Solution at the 1T stage $t_{\rm eq} < t < \infty$ is

$$T(r, t) = \frac{E_{\rm abs}}{\pi c d_f\, (R_{\rm eff}^2 + 4\chi_{2T} t_{\rm eq} + 4\chi(t - t_{\rm eq}))} \exp\left(-\frac{r^2}{R_{\rm eff}^2 + 4\chi_{2T} t_{\rm eq} + 4\chi(t - t_{\rm eq})}\right) + 300.$$

This is the two steps solution corresponding to the lateral conduction at the 2T and after that at the 1T stages. It describes relatively slow (it is slow at the 1T stage $t_{\rm eq} < t < \infty$) spreading and cooling of an initially hot spot, see figure 2. To see that it is slow at the 1T stage relative to the 2T stage, compare the profiles for $t = 0$ and $t = 10$ ps in figure 2 describing 2T spreading and the profile for $t = 40$ ps corresponding to the 1T stage 30 ps after finishing of the 2T stage. We see that the 10 ps changes at the 2T stage are much larger than the 30 ps changes during 1T stage.

Figure 2 presents typical results for the case with the highest energy $E_{\rm inc} = 1.74$ nJ shown in figure 1. It is 50% above the threshold $E_{\rm thr} = 1.15$ nJ. Then according to expression we have $R_{\rm cup} = R_{\rm eff}\sqrt{\ln(E/E_{\rm thr})} \approx 0.64\, R_{\rm eff} \approx 350$ nm. Thus the cupola radius is significantly less than the radius $R_{\rm eff}$ defining the initial distribution of fluence. Compare also the radiuses of cupolas given at the vertical axis in figure 1 and the effective radius $R_{\rm eff}$ following from the slope. We

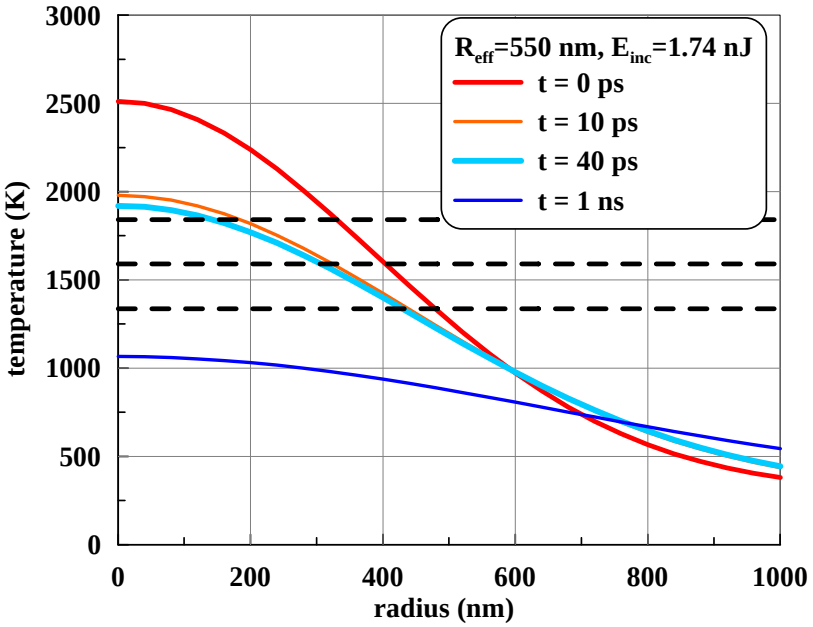

Figure 2. Evolution of the temperature distributions at the 2T stage beginning at $t = 0$ and ending at $t = 10$ ps and evolution at the 1T stage beginning at $t = 10$ ps. We see that the 2D 2T effects are appreciable, they in only 10 ps decrease equivalent ion temperature in the central region. While at the 1T stage the spreading of temperature is much slower. The case corresponds to the pulse with maximum energy 1.74 nJ in figure 3 and $R_{\text{eff}} = 550$ nm. If we define the cupola radius at the stage of separation $t \approx 40$ ps of a film from a substrate as the radius of a circle of molten gold then it approximately agree with a radius in figure 3 for this energy. Solid–liquid transition zone is shown by the horizontal straights 1337, 1590 and 1842 K, see text for explanations.

see that the experimental cupolas listed in figure 1 (black circles) are in the near threshold regime $0.19 < E/E_{\text{thr}} - 1 < 0.5$. Radiuses of the cupolas are extremely small thanks to (i) small wavelength $\lambda = 532$ nm (mainly λ defines R_{eff}), (ii) the tight focusing with a high numerical aperture NA technique, and (iii) using of the near threshold regime. As we see from figure 2, the cupolas only slightly overcome a melting conditions. Therefore the solid–liquid transition belt is wide and freezing is fast, even for the highest energy given in figure 1 it takes less than 1 ns to solidify liquid phase, see figure 2.

The straights in figure 2 approximately present the solid–liquid transition belt. To melt room temperature gold we have to heat it from 300 K to 1337 K and to add heat of fusion $E_m = 12.55$ kJ/mol $= 0.13$ eV/atom, $E_m/3k_B = 505$ K. In our heat conduction solution, freezing of molten gold begins when its temperature drops down to 1337+505=1842 K. Liquid phase totally solidifies when its temperature decreases to 1337 K. Of course, this is an approximate description of freezing more restricted than solution of a Stefan problem and than solutions given by the combined molecular dynamics (MD) and Monte-Carlo (MC) code (MD+MC), where deformation of a film and kinetics of freezing with strong overcooling of liquid below the melting temperature 1337 K are observed, see below. The middle line (1842+1337)/2=1590 K and the both limits 1842 K and 1337 K are shown in figure 2. They give estimates of a current boundary position between the molten and solid parts of a gold film.

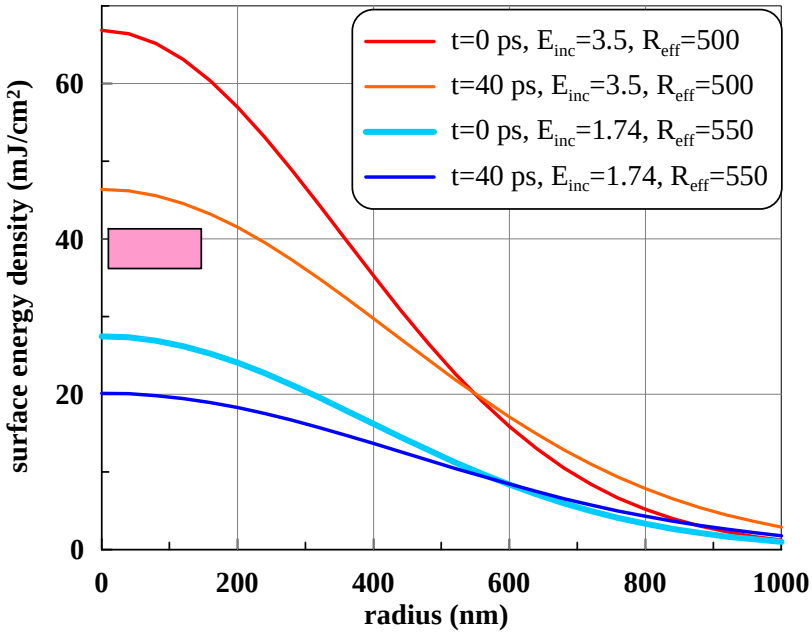

Figure 3. Local value of surface energy density F per unit area defines pressure acting at a contact between gold film and a glass substrate. Thus this value defines local velocity of a local center of mass (on a radius r) of a film after separation of a film from substrate. Due to the lateral spreading of heat at the stage of separation $0 < t < t^{\rm sep} \sim t_s$, $t^{\rm sep} \approx 40$ ps, the local value F changes with time. Therefore two profiles at the instant $t = 0$ and at the separation instant $t = 40$ ps are presented. Values $F \approx 15$–20 mJ/cm^2 correspond to a melting threshold, compare this figure and figure 2. The rectangular marks another threshold. Above this threshold an internal rupture of a film takes place, see text. The blue curves are connected with the black circle in figure 1 with the highest energy $E_{\rm inc}$ in the set of circles. The case with a moderately higher concentration of F (than that given by the blue curves) is also shown—the red curves.

3. Heating, melting, and dynamical behavior

It is more easy to stretch a liquid film than a solid film. Therefore the boundary of a molten circle gives us an estimate of an edge of an inflated cupola. But at what instant the position of a melting front defines the edge of cupola? Position of the edge is defined by an instant of separation. A film separates from substrate under action of pressure acting onto a film from substrate [11,12] after coming of a laser pulse. Pressure accelerates a film in the vacuum direction while the film is in mechanical contact with a substrate. A center of mass of a local piece of a film accumulates a normal component of momentum under action of this pressure because at the vacuum boundary of a film the pressure is zero. The separation process lasts $t^{\rm sep} \approx 40$–50 ps. Its duration is of the order of an acoustic time scale $t_s = d_f/c_s$, where c_s is speed of sound in gold. Therefore the instant $t = 40$ ps is presented in figure 2 and 3.

figure 4 presents extension of studies carried in [11, 12]. In [11, 12] the separation regime $F^{\rm sep} < F < F^{\rm rup}$ has been considered. Here we add the investigation of the rupture threshold $F^{\rm rup}$ and the investigation of the motions for the over threshold values $F > F^{\rm rup}$. The internal rupture of a film is a well known phenomenon in the case of a freestanding film when the both boundaries are boundaries with vacuum. But it seems that it is studied for the first time in the case of a film/substrate target. Due to a finite acoustic impedance of a substrate $Z_{\rm glass}$, the last case is asymmetric relative to the symmetric case of a thin homogeneously heated freestanding film when impedances $Z_{\rm vac}$ of the both media surrounding a film are equal (both are zero). For

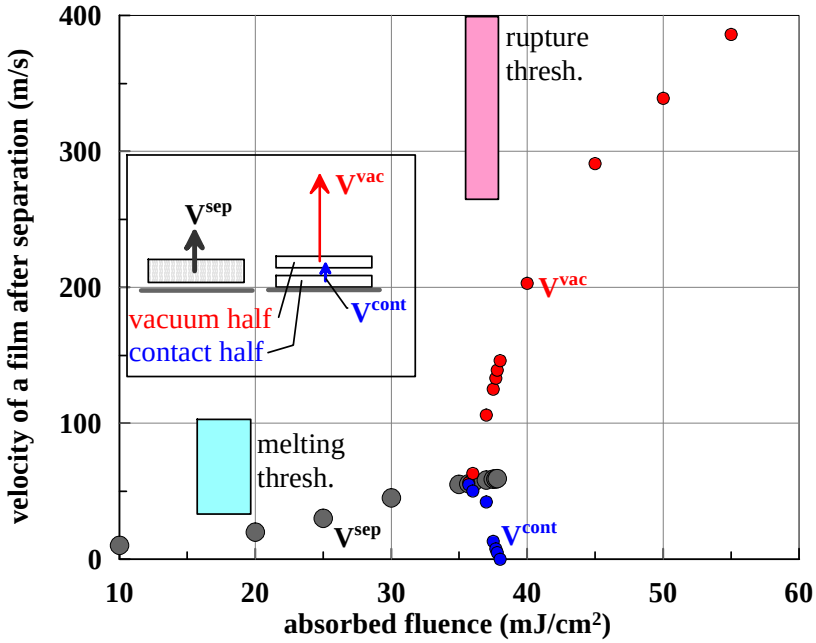

Figure 4. Dependence of separation velocity on absorbed fluence $F_{\rm abs}$. This is results of one-dimensional two-temperature hydrodynamics simulations for a sequence of values $F_{\rm abs}$. A gold film weakly coupled (small cohesion stress $p_{\rm coh} = 0.2$ GPa connecting gold and silica) to a glass (silica) substrate has been considered. Thickness of a film is 60 nm. This thickness is 10 nm larger than used in experiments presented in figure 1. The inset shows two regimes of motion. In the first regime $F^{\rm sep} < F < F^{\rm rup}$ a film delaminates as whole from a substrate with velocity $v^{\rm sep}$. In the second regime $F^{\rm rup} < F$ there are two parts of a film appearing after rupture of a film. These parts are the vacuum side subfilm and the contact side subfilm. Their centers of mass move with different velocities $v^{\rm vac}$ and $v^{\rm cont}$.

the gold–glass target the ratio of gold to glass impedances is large $Z_{\rm gold}/Z_{\rm glass} \approx 7$ [5.6]. Thus the situation is only slightly deviates from the freestanding film (glass in this sense slightly deviates from vacuum: $Z_{\rm gold} \gg Z_{\rm vac}$, $Z_{\rm gold} \gg Z_{\rm glass}$), and asymmetry of the rupture flow is small: the rarefaction from the contact side is weaker than the rarefaction from the vacuum side, therefore near the rupture threshold $F > F^{\rm rup}$ the contact subfilm is thinner than the vacuum subfilm shown in inset in figure 4.

In the silver–glass case the ratio of impedances 4.4 is significantly less than in the gold–glass case. Thus the asymmetry is larger. Pressures created in gold and silver are approximately the same at the same absorbed fluence and equal thicknesses d_f because both Gruneisen parameters Γ are near 2. Velocity of the vacuum boundary in a rarefaction wave $v_{\rm rw} = (\Gamma F_{\rm abs}/d_f)/Z$ is 50% higher for silver. For $F_{\rm abs} = 40$ mJ/cm^2 these velocities are 270 m/s for gold and 420 m/s for silver. As was shown in [11,12] the separation velocity $v^{\rm sep}$ in figure 4 is very significantly smaller than the rarefaction velocities $v_{\rm rw}$: $v^{\rm sep} \approx v_{\rm rw}/(Z_{\rm film}/Z_{\rm substr})$. This is a result of compensation of expansions into vacuum and into a "soft" ("almost vacuum") ($Z_{\rm substr} \ll Z_{\rm film}$) substrate—let us remember that velocity $v^{\rm sep}$ is an integral over thickness of a film—this is velocity of a center of mass. Velocity $v^{\rm sep}$ is nonzero due to a weak asymmetry of expansions. For $F_{\rm abs} = 40$ mJ/cm^2 the separation velocities $v^{\rm sep}$ are ≈ 40 m/s for gold and ≈ 100 m/s for silver.

Separate study is necessary to find the rupture threshold $F^{\rm rup}$ for the silver–glass target. If cohesion between film and substrate is weak $p_{\rm coh} \sim 0.2$ GPa then the separation threshold $F^{\rm sep}$ is rather small—few mJ/cm^2. A metal film separates into two parts—the vacuum and the contact

sides parts, see inset in figure 4. This takes place above the rupture threshold $F > F^{\rm rup}$. The rupture is a process beginning with nucleation in the middle layer of a film stretched by a tensile stress. After arrival of a femtosecond pulse a film waits for nucleation during an acoustic time scale while the rarefaction waves run through a film and reflect from the opposite boundaries. Duration of the rupture is shorter if the excess $F-F^{\rm rup}$ above the threshold is larger. At the end of the process of rupture, the vacuum and contact parts in inset in figure 4 lose their mechanical connection. After that the deceleration is finished and velocity of a center of mass of the vacuum subfilm does not change in time.

Close to the threshold $F > F^{\rm rup}$ the difference in velocities $v^{\rm vac}$ and $v^{\rm cont}$ of the subfilms in figure 4 is small- the cohesion stresses (resisting to the stretching of condensed matter inside a continuous film) almost totaly dump and decelerate stretching. Thus close to the threshold $F > F^{\rm rup}$ the velocities $v^{\rm vac}$ and $v^{\rm cont}$ in figure 4 slightly differ from velocity $v^{\rm sep}$ accumulated thanks to repulsion action of a substrate onto a film. The difference in velocities $v^{\rm vac}$ and $v^{\rm cont}$ in figure 4 quickly increases as the excess $F-F^{\rm rup}$ increases. There is only the short range of fluences in figure 4 where the contact subfilm flies out from the substrate. Above this range the contact subfilm remains on a substrate according to the two-temperature hydrodynamics simulations and according to our analytical acoustic model. If finally the contact subfilm somehow separates from a substrate this will be a result of much later processes taking place long after the stage of the acoustic interaction between a film and a substrate on an acoustic time scale defined by thickness of a film.

Figure 3 presents comparison between the energy concentration given by the highest black circle in figure 1 and the enhanced concentration with twice larger energy $E_{\rm inc}$ and 10% smaller effective radius $R_{\rm eff}$. We see that the internal rupture threshold is somewhere between these two concentrations. The threshold $F^{\rm rup}$ and values of velocities $v^{\rm sep}$ and $v^{\rm vac}$ are significant for us. As was shown above, the surface energy distribution $E_{\rm inc}(r)$ defines separation velocities $v^{\rm sep}$. Below we will see that the velocity distribution $v^{\rm sep}(r)$ together with a freezing process define a final shape of a solidified cupola. Our study is based on the link connecting $v^{\rm sep}(r)$ and the final shape of a bump. Using this link we will compare the experimentally measured (by atomic force microscope, AFM) shapes with calculations. Our task is to connect by calculations the experimental energy distribution $E_{\rm inc}(r)$ from one side and the experimentally observed shape from the other side. Let's present the simulations describing inflation of a bump and its freezing before we will proceed with the energy/shape connection.

4. Molecular dynamics and Monte-Carlo heat transport

The MD+MC code is used to follow evolution of a bump up to its freezing. Figure 5 illustrates the evolution. At the initial stage lasting $\sim$ 10 ps a film is melted by a thermostat and a velocity field directed normally to the surface is imposed. After that during the simulation run, in the periphery region the temperature $T_{\rm th}$ below a melting temperature of gold $T_{\rm th} < 1337$ K is supported by a thermostat localized in the periphery. The periphery region is the region between the simulation box $L_b \times L_b$ and the circle $r = L_b/2 - \Delta$. The rectangular $L_b \times L_b$ is a cross section of the box in the plane of initial film. The thermostat supports temperature $T_{\rm th}$ and does not allow the film to separate from substrate in the periphery region. Thus the condition of cohesive binding of a film to substrate outside a cupola is fulfilled. The momentum of a flying cupola gradually is transmitted to a substrate through the surface tension in a liquid part, through a tensile stress resisting to stretching in a solid part, and finally by the mechanical binding to the substrate. This chain of stresses decelerates motion of a bump at the stage when the bump flies out from a substrate. MC subroutine in the MD+MC code is responsible for cooling of a bump thanks to electron heat conduction along a metal film.

The sizes used in the simulation shown in figure 5 are: $L_b = 270$ nm, $\Delta = 5$ nm, initial thickness d_{f0} of a film is 10 nm. Other parameters are: coefficient of heat conduction is $\kappa = 42$

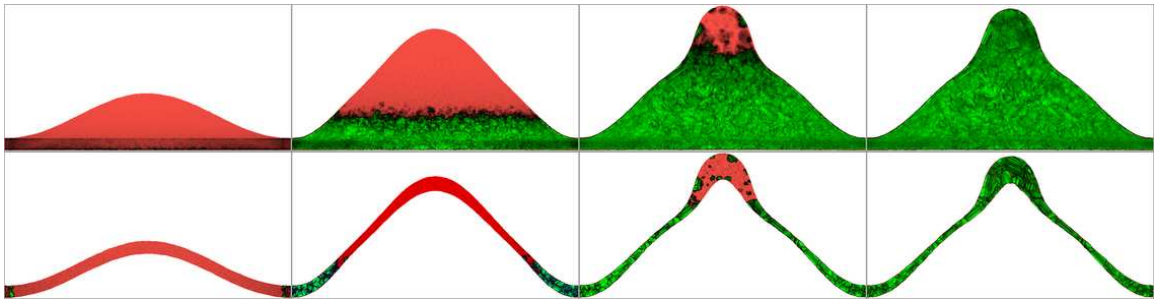

Figure 5. Evolution of cupola according to MD+MC simulation. Time instants are: 0.216 ns, 0.648 ns, 1.296 ns, and 2.34 ns. Initial velocity field was $v(r) = v_c(0)\cos^2[\pi r/(L_b - 2\Delta)]$, $v_c(0) = 200$ m/s. Green colors correspond to the solidified gold, while red color—to a liquid phase. We see how the recrystallization gradually proceeds along the bump.

W/m/K, surface tension is $\sigma = 540$ dyn/cm. This is a coefficient of surface tension in the interatomic potential used in MD simulation. There are two main nondimensional parameters ruling the flow. They are the capillary and thermal numbers

$$v_{0\sigma} = v_c(0)/v_\sigma, \quad v_\sigma = 2\sqrt{\sigma/(\rho_0 d_{f0})},$$
$$v_{0\chi} = v_c(0)/v_\chi, \quad v_\chi = \chi/R_{\rm cup}, \quad \chi = \kappa/c, \quad c = 3k_B n_0,$$

here $v_c(r = 0)$ is initial velocity of a film in its tip point after separation from substrate, ρ_0, n_0 are initial density and atomic concentration. For the simulation shown in figure 5 these values are: $v_c(0) = 200$ m/s, $v_\sigma = 106$ m/s, $v_{0\sigma} = 1.9$, $v_\chi = 130$ m/s, $v_{0\chi} = 1.5$.

In the experiment we have $\sigma \approx 1000$ dyn/cm, $d_{f0} = 50$ nm, $v_\sigma = 64$ m/s, and $\chi \approx 1.2$ cm^2/s, $v_\chi = 220$ m/s. Cooling velocity v_χ for experiment is calculated as $\chi/R_{\rm eff}$ with $R_{\rm eff} = 550$ nm from figures 3, 4. We do so because in experiment a temperature gradient is defined by a radius $R_{\rm eff}$ which for the sequence of the black circles in figure 3 is significantly larger than the radius of cupola. While in the MD+MC simulation we support fixed temperature in the periphery area thus the radius $R_{\rm cup} = L_b/2 - \Delta$ is more appropriate to put into expression for v_χ; $R_{\rm cup} = 270/2 - 5 = 130$ nm for figure 5.

5. Thin shell model

Let's use a model of thin shell from papers [11, 12]. Corresponding code is much faster in comparison with the MD+MC code. In non-dimensional variables $\hat r, \hat z, \hat t$ system of equations is

$$\frac{\partial^2 \hat r}{\partial \hat t^2} = -C\,\frac{\partial \hat z}{\partial \hat a}, \quad \frac{\partial^2 \hat z}{\partial \hat t^2} = C\,\frac{\partial \hat r}{\partial \hat a},$$
$$\hat R = k^3/(\hat z''\hat r' - \hat r''\hat z'), \quad k = \sqrt{\hat r'^2 + \hat z'^2},$$
$$\hat r' = \frac{\partial \hat r}{\partial \hat a}, \quad \hat z' = \frac{\partial \hat z}{\partial \hat a}, \quad C = \frac{1}{2}\left(\frac{\hat r}{\hat a\,\hat R} + \frac{\hat z'}{k\,\hat a}\right),$$
$$\hat r = \frac{r}{R}, \quad \hat z = \frac{z}{R}, \quad \hat t = \frac{t}{(R/v_\sigma)}.$$

Here r, z are cylindrical coordinates—radius and height.

6. Conclusion

An action of an ultrashort (subpicosecond) laser pulse onto a thin ($d_f = 30$–70 nm) gold film deposited on a glass substrate is considered. Consideration includes analysis of absorption of

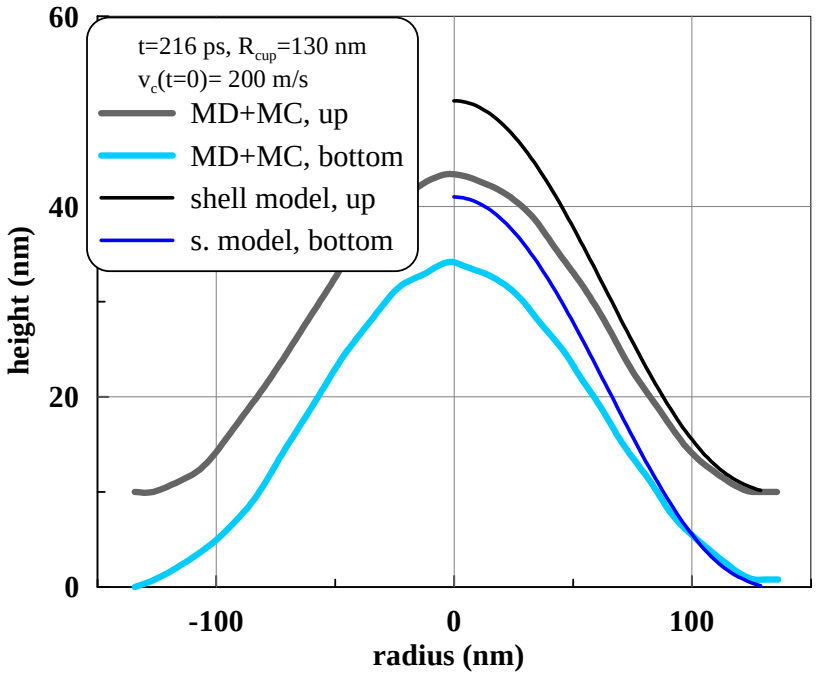

Figure 6. Calculation based on the thin shell model for initial data corresponding to the MD+MC run shown in figure 5. Comparison is made at the instant $t = 216$ ps. The model gives 19% higher cupola. This seems is a result of a finite thickness of the cupola in the MD+MC run $d_{f0}/R_{\rm cup} = 0.08$.

laser energy and heat conductivity effects together with numerous dynamical effects. High electron heat conductivity during very short time less than one picosecond homogeneously distributes absorbed energy across a thickness of a thin film (i.e., normally to the surface). After that the lateral heat conduction effects become significant. They are especially significant for the tight focusing case when an irradiated focal spot is less than micron in diameter and during the 2T stage when there are enhanced values of heat diffusion coefficient. Lateral conduction is less significant on acoustic time scale after finishing of the 2T stage.

It is shown that for thin films ($d_f = 30$–70 nm) an acoustic time scale $t_s = d_f/c_s \sim 10$–20 ps is comparable with duration of a 2T stage 10–20 ps in gold. Lateral heat conduction at the 1T stage is very important ingredient of the physical picture of blistering but at much longer time scale from few to few tens and more nanoseconds. Lateral cooling is important because it is responsible for cooling of gold molten inside the irradiation spot. Cooling of liquid (typical temperatures are less than ≈ 3 kK for thin films in the cases interesting for us) is dynamically almost insignificant since viscous and Marangoni effects are small in our flows with a flying cupola-like shell. But freezing changes dynamical situation qualitatively because it suppress extensibility of the liquid film forming the cupola-like shell.

It is shown above that the combination of cooling/freezing with inertia of flying mass and with capillarity phenomena successively explains diverse morphology of the solidified structures obtained on a thin film under ultrashort diffraction limited illumination. Developed above computational techniques include 2T hydrodynamics code, thin film model, and molecular dynamics with Monte-Carlo simulation code.

Acknowledgments
This work was supported by the Russian Science Foundation (grant 14-19-01599, for V V Zh, V A Kh and N A I).

Appendix. Corresponding program (mathematica)

```
r = rr[a,t]; z = zz[a,t];
rtt = D[r, {t,2}]; ztt = D[z, {t,2}];
ra = D[r, a]; za = D[z, a];
raa = D[r, {a,2}]; zaa = D[z, {a,2}];
k = Sqrt[ra^2+za^2]; R = k^3/(zaa ra - raa za);
Cu = (1/2)( 1/R + za/(r + 10^-7 )/
 (k + 10^-7 ) ) r/( a + 10^-7 );

eqr = rtt + Cu za;  eqz = ztt - Cu ra;

sol=  NDSolve[{eqr==0, eqz==0,
  rr[a,0]==a, zz[a,0]==0,
  (D[rr[a,t],t]/.t->0)==0,
  (D[zz[a,t],t]/.t->0) == hatV Cos[ Pi a/2 ]^2,
 rr[0,t]==0, (D[zz[a,t],a] /. a->0)  ==  0,
 rr[ 1, t] == 1,    zz[ 1, t] == 0 }, {rr, zz},
    {a, 0, 1 },  {t, 0, tEND  }  ]

 rrr[a_,t_] = Evaluate[rr[a, t] /. sol];
 zzz[a_,t_] = Evaluate[zz[a, t] /. sol];
vr[a_,t_] = D[rrr[a, t], t];
ACCr[a_,t_] = D[rrr[a, t], {t,2} ];
vz[a_,t_] = D[zzz[a, t], t];
ACCz[a_,t_] = D[zzz[a, t], {t,2} ];
rra[a_, t_] = D[rrr[a, t], a];
zza=D[zzz[a, t], a];
dsda[a_, t_] = Sqrt[ rra[a, t]^2 + zza^2 ];

 Plot[zzz[a, 0.51], {a, 0, 1}]
 ZRhatV19 =
  Table[{i, rrr[i, .51], zzz[i, .51]},
    {i, 0, 1, 1/100.}]
 Save["c:\0_ZRv19t051.dat", ZRhatV19]
```

References

[1] Korte F, Koch J and Chichkov B N 2004 *Appl. Phys.* A **79** 879
[2] Ivanov D S, Kuznetsov A I, Lipp V P, Rethfeld B, Chichkov B N, Garcia M E and Schulz W 2013 *Appl. Phys.* A **111** 675
[3] Nakata Y, Okada T and Maeda M 2003 *Jpn. J. Appl. Phys.* **42** L1452
[4] Gubko M A, Husinsky W, Ionin A A, Kudryashov S I, Makarov S V, Nathala C R, Rudenko A A, Seleznev L V, Sinitsyn D V and Treshin I V 2014 *Laser Phys. Lett.* **11** 065301
[5] Ivanov D S and Zhigilei L V 2003 *Phys. Rev.* B **68** 064114
[6] Povarnitsyn M E, Itina T E, Sentis M, Khishchenko K V and Levashov P R 2007 *Phys. Rev.* B **75** 235414

[7] Inogamov N A, Zhakhovskii V V, Ashitkov S I, Petrov Yu V, Agranat M B, Anisimov S I, Nishihara K and Fortov V E 2008 *J. Exp. Theor. Phys.* **107** 1–19
[8] Povarnitsyn M E, Itina T E, Khishchenko K V and Levashov P R 2009 *Phys. Rev. Lett.* **103** 195002
[9] Loboda P A, Smirnov N A, Shadrin A A and Karlykhanov N G 2011 *High Energy Density Phys.* **7** 361–370
[10] Wu C, Christensen M S, Savolainen J M, Balling P and Zhigilei L V 2015 *Phys. Rev.* B **91** 035413
[11] Inogamov N A and Zhakhovskii V V 2014 *JETP Lett.* **100** 4–10
[12] Inogamov N A, Zhakhovskii V V and Khokhlov V A 2015 *J. Exp. Theor. Phys.* **120** 15–48
[13] Babar S and Weaver J 2015 *Appl. Optics* **54** 477–481
[14] Inogamov N A, Zhakhovskii V V, Ashitkov S I, Khokhlov V A, Shepelev V V, Komarov P S, Ovchinnikov A V, Sitnikov D S, Petrov Yu V, Agranat M B, Anisimov S I and Fortov V E 2011 *Contrib. Plasma Phys.* **51** 367–374